metals

MDPI

Article

Strain Hardening Exponent and Strain Rate Sensitivity Exponent of Cast AZ31B Magnesium Alloy

Yanchun Zhu [1,2], Qinghua Wang [1,2], Zhiquan Huang [1,2,*], Ling Qin [3], Ziliang Li [1] and Lifeng Ma [1,2]

[1] School of Mechanical Engineering, Taiyuan University of Science and Technology, Taiyuan 030024, China
[2] Institute of Heavy Equipment Machine Intelligence, Taiyuan University of Science and Technology, Taiyuan 030024, China
[3] Department of Engineering, University of Hull, Cottingham Rd, Hull HU6 7RX, UK
* Correspondence: w20220416@126.com

Abstract: The flow curves of as-cast AZ31B magnesium alloy during high temperature deformation were obtained with a thermal compression test, and the effects of deformation amount, grain size, strain rate, and deformation temperature on the flow stress, strain rate sensitivity index, and strain hardening index were analyzed. The results showed that deformation and grain size were negatively correlated with both the strain rate sensitivity index and strain hardening index. The increase in strain rate increased the strain hardening index but made the strain rate sensitivity index show an opposite trend. Increasing temperature reduced the strain rate sensitivity index and strain hardening index but, when the temperature exceeded 700 K, the strain rate sensitivity index was no longer affected by temperature. Since the strain rate sensitivity index m and strain hardening index n are important parameters for measuring the plastic deformation of metal materials, this study has great significance for guiding the selection of process parameters in the plastic processing of as-cast AZ31 magnesium alloy.

Keywords: as-cast AZ31B magnesium alloy; rheological behavior; strain rate sensitivity index; strain hardening index; microstructure

check for updates

Citation: Zhu, Y.; Wang, Q.; Huang, Z.; Qin, L.; Li, Z.; Ma, L. Strain Hardening Exponent and Strain Rate Sensitivity Exponent of Cast AZ31B Magnesium Alloy. *Metals* **2022**, *12*, 1942. https://doi.org/10.3390/met12111942

Academic Editors: Frank Czerwinski and Marcello Cabibbo

Received: 14 September 2022
Accepted: 7 November 2022
Published: 12 November 2022

Publisher's Note: MDPI stays neutral with regard to jurisdictional claims in published maps and institutional affiliations.

Copyright: © 2022 by the authors. Licensee MDPI, Basel, Switzerland. This article is an open access article distributed under the terms and conditions of the Creative Commons Attribution (CC BY) license (https://creativecommons.org/licenses/by/4.0/).

1. Introduction

With the increase in fuel costs, the demand for lightweight automobiles is growing more and more. Magnesium alloy is the lightest metal structural material at present. Compared with steel and aluminum alloys, magnesium alloy has the advantages of low density, high specific strength and specific stiffness, good thermal conductivity and damping, good electromagnetic shielding performance, easy cutting, and the capacity to be recycled. Based on these advantages, it has broad application prospects in the aerospace, transportation, electronic communication, and home appliance industries [1–3]. However, magnesium alloy has a hexagonal, close-packed crystal structure, which leads to a weaker start-up slip system and poor plastic deformation ability during deformation at room temperature, severely limiting its practical applications [4,5].

It is well-known that the strain rate sensitivity index m and strain hardening index n are important parameters for measuring the plastic deformation of metal materials. The strain rate sensitivity index m is the parameter for the material's tendency toward strengthening when the strain rate changes; the strain hardening exponent n is the parameter that describes the work hardening behavior of metal materials during deformation and reflects the ability of materials to resist plastic deformation. Therefore, it is of great significance to study the responses of the strain rate sensitivity index m and strain hardening index n of magnesium alloy to process parameters and microstructure changes during isothermal compression.

Wang et al. [6] studied the strain rate sensitivity and anisotropic behavior of a rare-earth magnesium sheet alloy ZEK100 and found that the strain rate sensitivity of the ZEK100 sheet depended strongly on both the loading orientation and the strain amplitude.

E. Karimi et al. [7] studied the instantaneous strain rate sensitivity of wrought AZ31 magnesium alloy and found that the instantaneous strain rate sensitivity of the AZ31 alloy was significantly affected by the strain rate and imposed strain. N. Sriraman et al. [8] determined the different stages of strain hardening exhibited by variously processed Mg-4Li-0.5Ca alloy test specimens and discovered that, after more plastic strain (dislocation density) was accumulated in the KAM [9] mapping, the AR350 alloy exhibited a higher strain hardening rate in the later stage.

Although research on the strain rate sensitivity index and strain hardening index has begun to increase in recent years, most studies are not systematic enough. This study took as-cast AZ31B magnesium alloy as the research object and analyzed the influence of different process variables on flow stress, calculated the strain rate sensitivity index m and strain hardening index n of as-cast AZ31B magnesium alloy under different forming parameters, and analyzed the influence of microstructure and process parameters on the two indexes. This has important theoretical significance and engineering value for improving the material properties of as-cast AZ31B magnesium alloy, making it possible to improve the process to optimize the microstructure.

2. Experiment

2.1. Experimental Materials

The experimental raw material was a casting billet of AZ31B magnesium alloy produced by a company. The original microstructure is shown in Figure 1. It can be seen that the microstructure of as-cast AZ31B magnesium alloy is composed of irregular original coarse grains, the crystal boundary is clear, and fine recrystallized grains appeared at the grain boundaries of some large grains. The chemical constituents of the material are shown in Table 1.

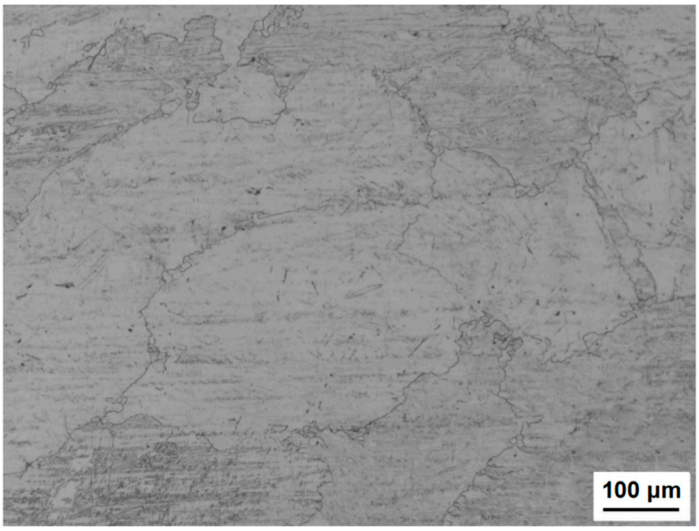


Figure 1. The original microstructure of AZ31B alloy.

Table 1. Composition of AZ31B (wt.%).

Al	Zn	Mn	Si	Fe	Cu	Ca	Be	Mg
3.19	0.81	0.334	0.02	0.005	0.05	0.04	0.1	Bal.

2.2. Experimental Procedures

Generally, there are three methods used to study the thermal deformation behavior of materials: uniaxial tension, uniaxial compression, and torsion. Figure 2 shows the process for the compression simulation experiment. In this experiment, the uniaxial compression process of AZ31 magnesium alloy under a series of different temperatures and strain rates was simulated with a Gleeble−3800 compression testing machine from Fleur Instrument

Technology (Shanghai) Co., Ltd., China. The flow stress data for the material during hot compression were automatically collected and recorded by the computer of the thermal simulator of the testing machine. The compressed specimen used in this study was a cylindrical standard test sample processed by WEDM (specification: Φ8 × 12 mm) from Suzhou AVIC Technology Equipment Co., Ltd., China. Lubricants (graphite and oil) were coated on the two ends of the specimen to reduce the friction between the punch and the sample and avoid uneven deformation. Since magnesium alloy has an HCP(hexagonal closepacked structure) structure, the formability is poor at room temperature and increases significantly with increasing temperature. It is known that most wrought magnesium alloys have good formability at high temperatures of 623~773 K ([10,11]) and that the deformation of magnesium alloy is affected by stress state and alloy structure ([12–14]). Therefore, the compression deformation temperature range was set to 623–773 K; the strain rates were 0.1 s^{-1}, 1 s^{-1}, and 10 s^{-1}; and the compression amount was 60% After the experiment, the samples were cooled to room temperature in air; 400#, 800#, 1000#, 1500#, 2000#, and 3000# water-grinding sandpaper was used to grind the metallographic samples; and a mixed solution composed of 5 g picric acid + 5 g glacial acetic acid + 10 mL distilled water + 80 mL anhydrous ethanol was used to erode the polished metallographic samples. Then, the microstructures of the samples were observed with an optical microscope.

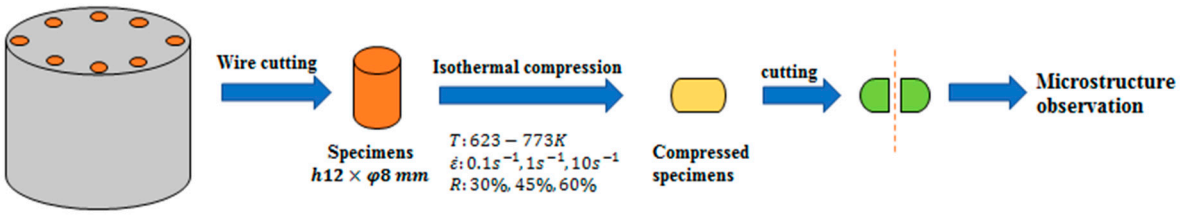


Figure 2. Schematic diagram of the experimental process.

Following this, in accordance with the flow stress data automatically recorded in the experiment, the change rule for the value of the strain rate sensitivity coefficient m with changes in temperature and strain rate and the change rule for the value of strain hardening coefficient n with changes in strain and temperature could be calculated.

3. Results and Discussion

3.1. Flow Behavior of the AZ31B Alloy

Figure 3 shows the typical true stress–strain curve of as-cast AZ31B magnesium alloy after hot compression, indicating the influence of different deformation conditions on the flow stress of AZ31B magnesium alloy under the condition of 60% deformation [15–17]. It can be seen that the change trend for the flow stress–strain curves of AZ31B magnesium alloy under different deformation conditions were similar; that is, in the initial stage of deformation, with the increase in strain, the flow stress increased rapidly and reached the peak stress, then decreased gradually, and, finally, tended toward stability. Researchers believe that the reasons for this phenomenon are as follows [18–20]. In the initial stage of deformation, strain hardening occupies a dominant position, so the flow stress increases with the increase of strain. However, with the deepening of deformation, the softening effect of dynamic recrystallization and dynamic recovery gradually increases, which gradually offsets the strain hardening effect, resulting in a slow decline in flow stress. When the dynamic recrystallization softening and strain hardening reach equilibrium, the flow stress acquires a stable state. In addition, the wavy stress–strain curves in Figure 3a,c should be derived from the electronics of the testing machine and did not affect the results discussed in this paper.

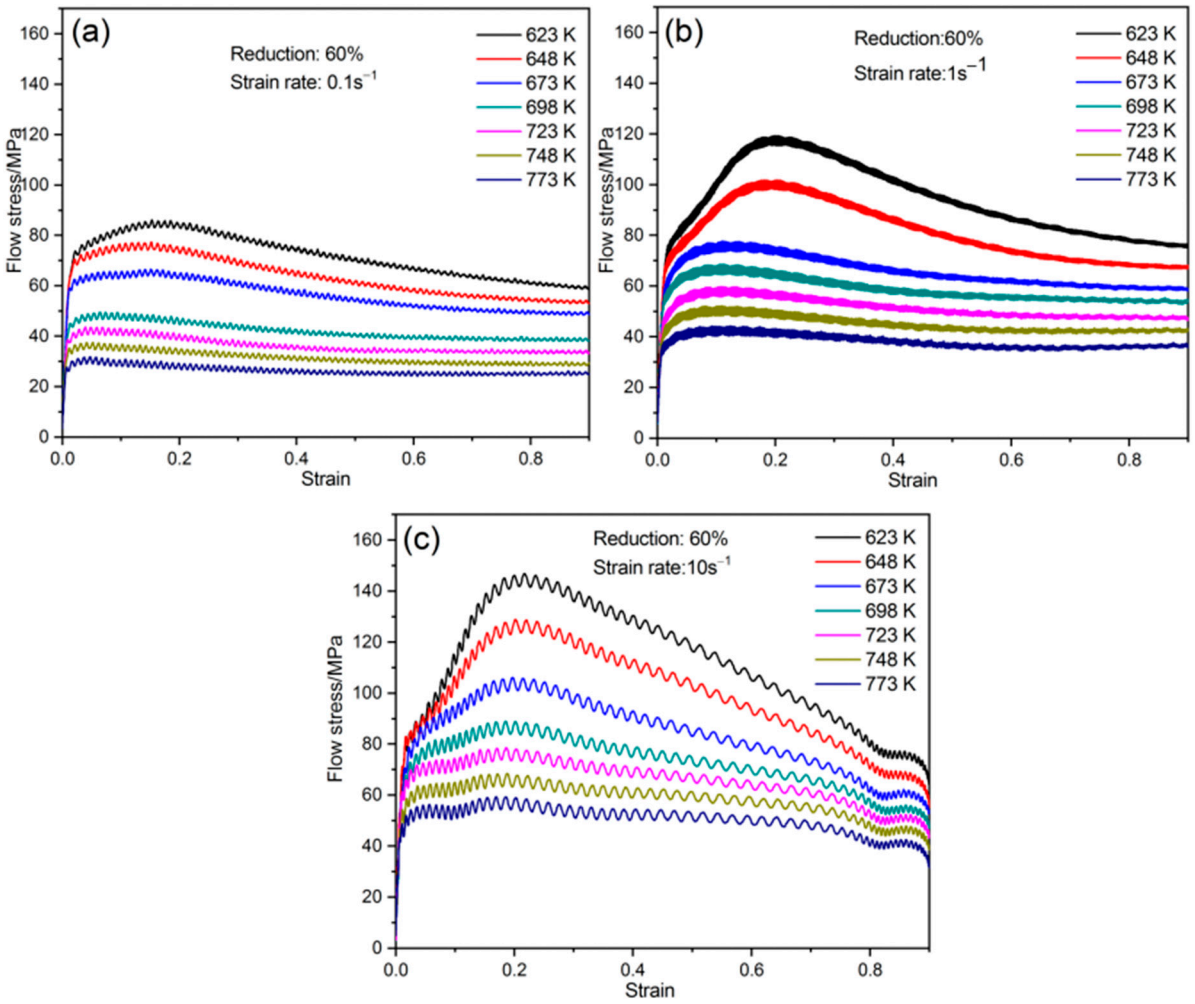


Figure 3. Typical flow stress–strain curves of as-cast AZ31B magnesium alloy: (**a**) $\dot{\varepsilon} = 0.1\ s^{-1}$; (**b**) $\dot{\varepsilon} = 1\ s^{-1}$; (**c**) $\dot{\varepsilon} = 10\ s^{-1}$.

We can intuitively and quickly discern from Figure 3 that the flow stress and its peak value for AZ31B magnesium alloy diminished gradually as the deformation temperature increased at a certain strain rate. The reason is that the essence of metal deformation is the process of fracturing and re-bonding of metal bonds. The higher the deformation temperature, the more kinetic energy the metal atoms obtain during deformation, so that the atoms are more likely to break away from the metal bonds to soften the metal materials; that is, the flow stress of the metal decreases, and the peak stress that needs to be overcome in the deformation decreases. At the same time, comparing Figure 3a–c, it can be seen that the flow stress of AZ31B magnesium alloy increased with the increase in the strain rate at the same deformation temperature. This was because, as the strain rate increases, the time required for the material to produce the same amount of deformation becomes shorter and shorter, so that the alloy does not have enough time to complete dynamic recrystallization, which means that the softening effect is not obvious and the work hardening effect is more and more significant, finally causing the increase in flow stress [21].

In summary, the flow stress of as-cast AZ31B magnesium alloy was highly sensitive to deformation temperature, strain rate, and strain.

Figure 4 displays the effects of deformation temperature and strain rate on flow stress under different strain conditions. On the whole, the flow stress of AZ31B magnesium alloy decreased gradually with the increase in the deforming temperature, which was due to the dynamic softening phenomenon in the material with the increase in deformation

temperature, and the dynamic softening of the material was sufficient to offset its strain hardening during isothermal compression [22].

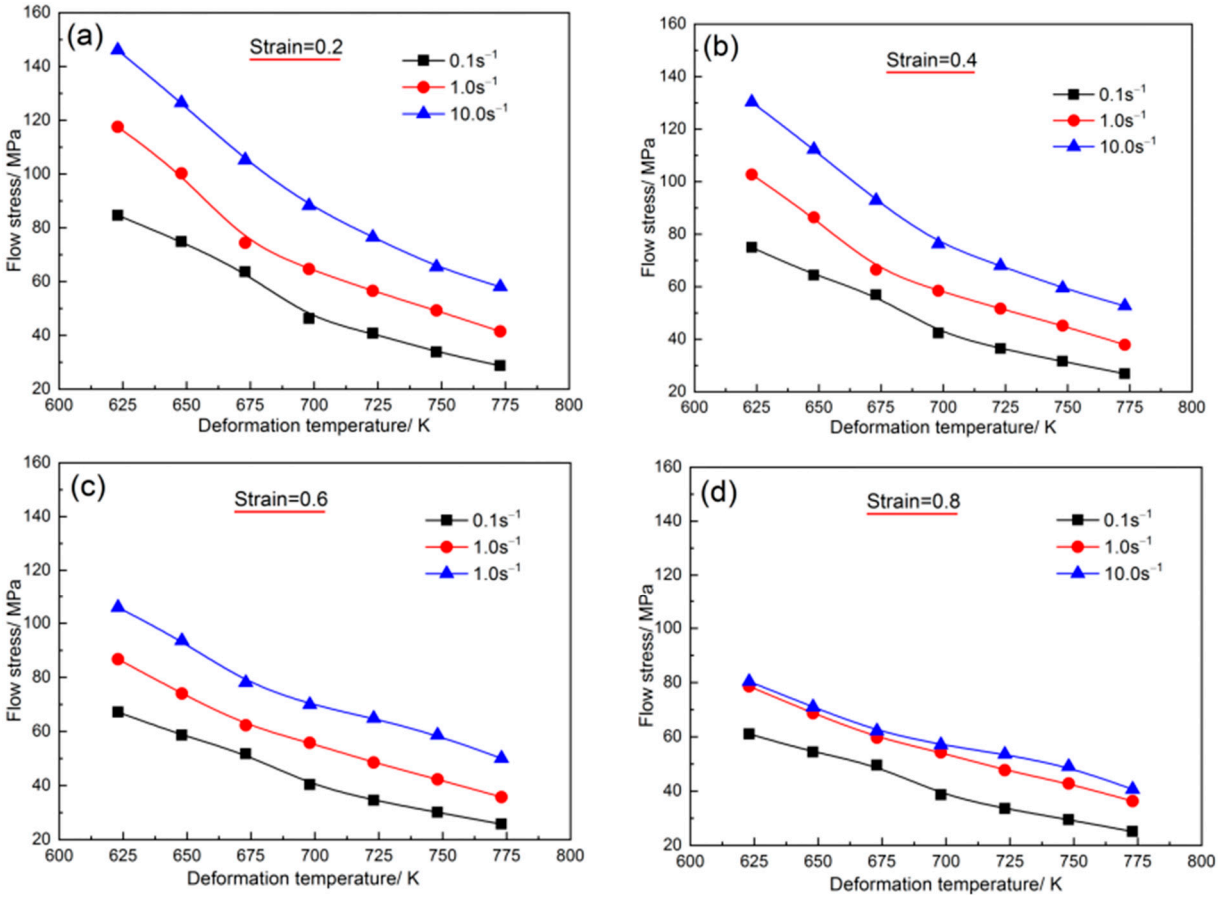


Figure 4. The variation trend for flow stress with strain rate and deformation temperature under different strain conditions: (**a**) $\varepsilon = 0.2$; (**b**) $\varepsilon = 0.4$; (**c**) $\varepsilon = 0.6$; (**d**) $\varepsilon = 0.8$.

The trend for the curve in Figure 4 shows that, under the same strain rate and deformation temperature, the flow stress of the alloy gradually decreased with the increase in the strain. This was due to the fact that, with the increase in strain, the original coarse grains in the microstructure of the alloy were completely crushed, and dynamic recrystallization occurred under the action of higher deformation temperature, which triggered the softening mechanism of recrystallization and led to the gradual decrease in the flow stress of the alloy. Meanwhile, we found that, under the same deformation conditions, as the strain rate increased, the flow stress of the alloy increased gradually. This was because the larger strain rate led to a shorter time being required for the material to complete the deformation, so the alloy did not have enough time to complete the nucleation and growth of dynamic recrystallization, resulting in the softening effect of dynamic recrystallization not being obvious. At this time, the strain hardening mechanism gradually occupied the dominant position, so the flow stress increased gradually with the increase in strain rate [23].

In addition, Figure 4 also shows that with the strain increase, the difference between the flow stress curves corresponding to the three strain rates in the figure became smaller and smaller, which was similar to the trend for the curve in the graph. This phenomenon shows that the increase in deformation led to the gradual dominance of recrystallization softening.

In general, the flow stress of the alloy gradually decreased with the increase in deformation temperature, and the higher the strain rate, the faster the flow stress decreased.

As can be seen in Figure 5, under the same deformation temperature, the flow stress of the alloy increased with the increase in strain rate, which was due to the strain hard-

ening phenomenon gradually offsetting the softening phenomenon caused by the high temperature deformation and occupying the dominant role in the increase in the strain rate, increasing the flow stress.

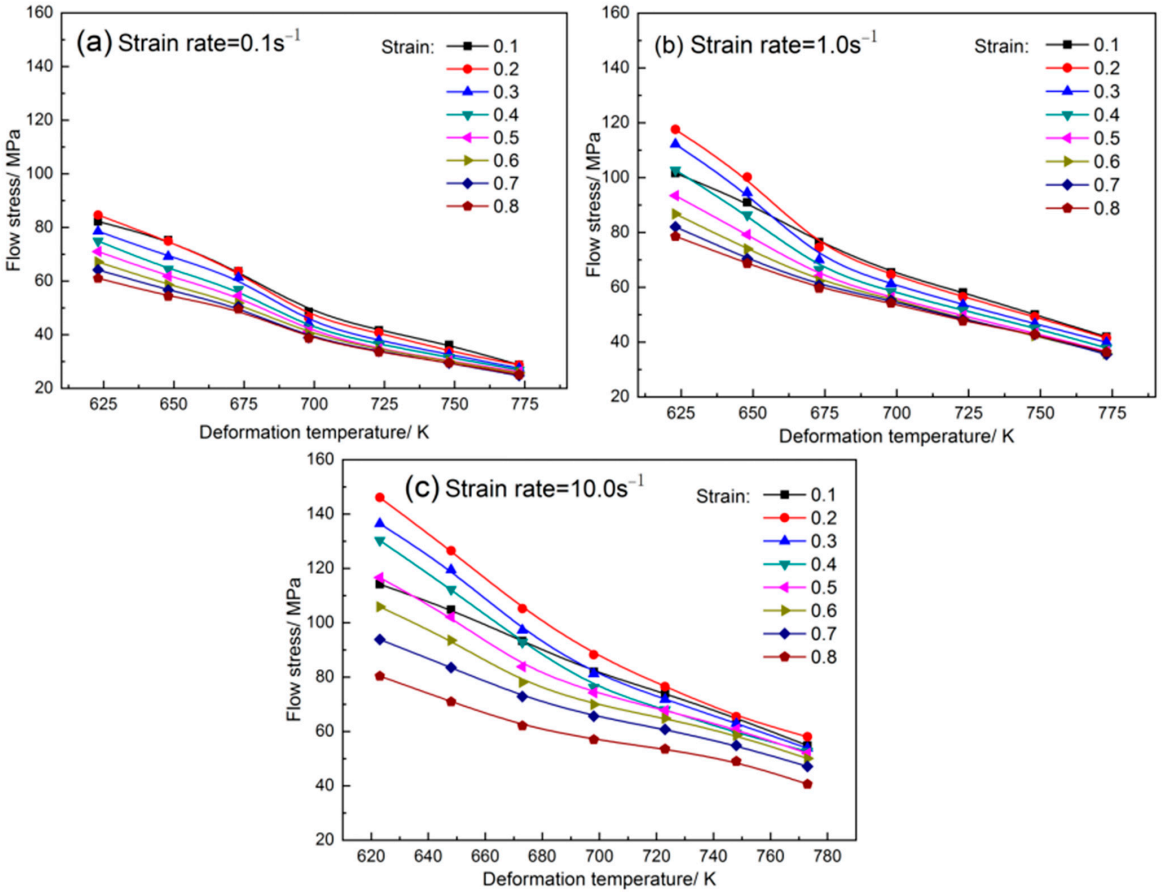


Figure 5. The variation trend for the flow stress with strain and deformation temperature under different strain rates: (**a**) $\dot{\varepsilon} = 0.1\ s^{-1}$; (**b**) $\dot{\varepsilon} = 1\ s^{-1}$; (**c**) $\dot{\varepsilon} = 10\ s^{-1}$.

In the case of low deformation temperature, there was a great difference in the flow stress values under different strains, while the difference gradually decreased with the increase in deformation temperature. The principle is as follows: with the increase in deformation temperature, atoms obtain more kinetic energy, making the dislocation movement easier and promoting the start of the dynamic softening mechanism in the material, which gradually occupies the dominant position, resulting in the decrease in flow stress [24].

3.2. Strain Rate Sensitivity Exponent

The strain rate sensitivity index m refers to the parameter for the sensitivity of the flow stress of the metal material to the strain rate when plastic deformation occurs; that is, the parameter for the strengthening tendency of the material when the strain rate increases. In this study, the strain rate sensitivity index was determined with the following expression [25]:

$$m = \left.\frac{d\log\sigma}{d\log\dot{\varepsilon}}\right|_{\varepsilon,T} \quad (1)$$

where m is the strain rate sensitivity index; σ is the flow stress (MPa) measured in the compression simulation experiment; $\dot{\varepsilon}$ is the strain rate (s^{-1}); ε is the strain; and T is the deformation temperature (K). It can be seen from Equation (1) that, when the strain and temperature are constant, the value of m is related to the strain rate and stress, and the size is negatively correlated with the strain rate and positively correlated with the stress.

In accordance with the experimental data from the thermal compression simulation, the $\ln\sigma - \ln\dot{\varepsilon}$ curves for strains of 0.2, 0.4, 0.6, and 0.8 were respectively fitted, and the corresponding mathematical expression was as follows:

$$\lg\sigma = a_1 + a_2\lg\dot{\varepsilon} + a_3(\lg\dot{\varepsilon})^2 \quad (2)$$

The values of their corresponding coefficients a1, a2, and a3 were obtained.

The strain rate sensitivity index m was obtained by derivation of $\ln\dot{\varepsilon}$ on both sides of the above formula, as follows:

$$m = \frac{\lg\sigma}{\lg\dot{\varepsilon}} = a_2 + 2a_3\lg\dot{\varepsilon} \quad (3)$$

The corresponding values of m were calculated with the above two formulas.

Assuming that the temperature was the x-axis, ln was the y-axis, and m was the z-axis, contour map 6 was drawn in Origin software. The m contour map reflects the change in strain rate sensitivity index m with temperature and strain rate (see the figure below).

The strain rate sensitivity is usually used to determine the superplastic behavior and deformation mechanism of materials. Figure 6 shows the variation trend for the strain rate sensitivity index m with strain rate and deformation temperature under different strain conditions.

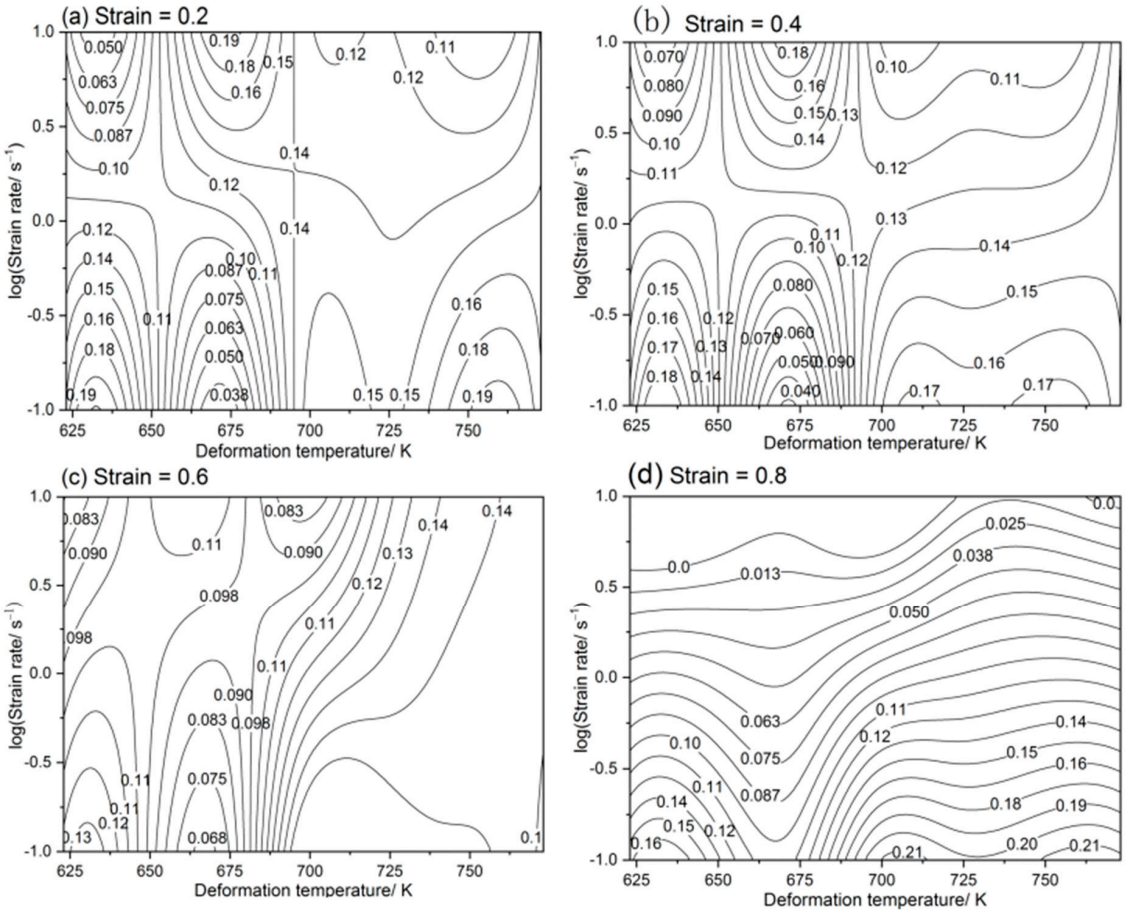


Figure 6. Contour map of strain rate sensitivity exponent of AZ31B mg alloy under different strain conditions: (**a**) $\varepsilon = 0.2$; (**b**) $\varepsilon = 0.4$; (**c**) $\varepsilon = 0.6$; (**d**) $\varepsilon = 0.8$.

Overall, with the increase in strain, the peak value of the strain rate sensitivity index decreased first and then increased. At the same time, the peak value of the strain rate sensitivity index of AZ31B magnesium alloy under different strain conditions almost appeared

in the low strain rate region, up to 0.21. This indicates that, in the plastic deformation stage, low strain rate and high strain were conducive to improving the strain rate sensitivity index. The reason is the low strain rate stage involves a long deformation time, and the material has enough time for dynamic recrystallization nucleation and growth; at the same time, the softening and hardening mechanisms of the material are fully initiated, which promotes the increase in strain rate sensitivity. This also provides some help and inspiration for the plastic processing of the material: in the plastic processing of magnesium alloy materials, the selection of the strain rate should be appropriate, especially for the selection of a high strain rate.

It can also be seen from Figure 6 that, when the strain value is constant, the strain rate sensitivity index m of AZ31B magnesium alloy gradually decreases with the increase in strain rate. This is because, as the strain rate increases, the time required for the same deformation of the metal materials becomes shorter and shorter, resulting in there being insufficient time for the metal materials to complete the nucleation and growth of dynamic recrystallization in the deformation process, leading to a gradual decrease in the strain rate sensitivity index. It was also found that, when the deformation temperature was greater than 700 K, it had little effect on the strain rate sensitivity index under the condition of constant strain rate. This phenomenon was more obvious when the strain was 0.8, and the contour line in the figure was almost parallel to the abscissa.

J. Luo et al. [26] pointed out that the alloy composition, grain size, and phase volume fraction also have some influence on the strain rate sensitivity index. Figure 7 shows the influence of different deformation conditions on the microstructure of AZ31B magnesium alloy during isothermal compression.

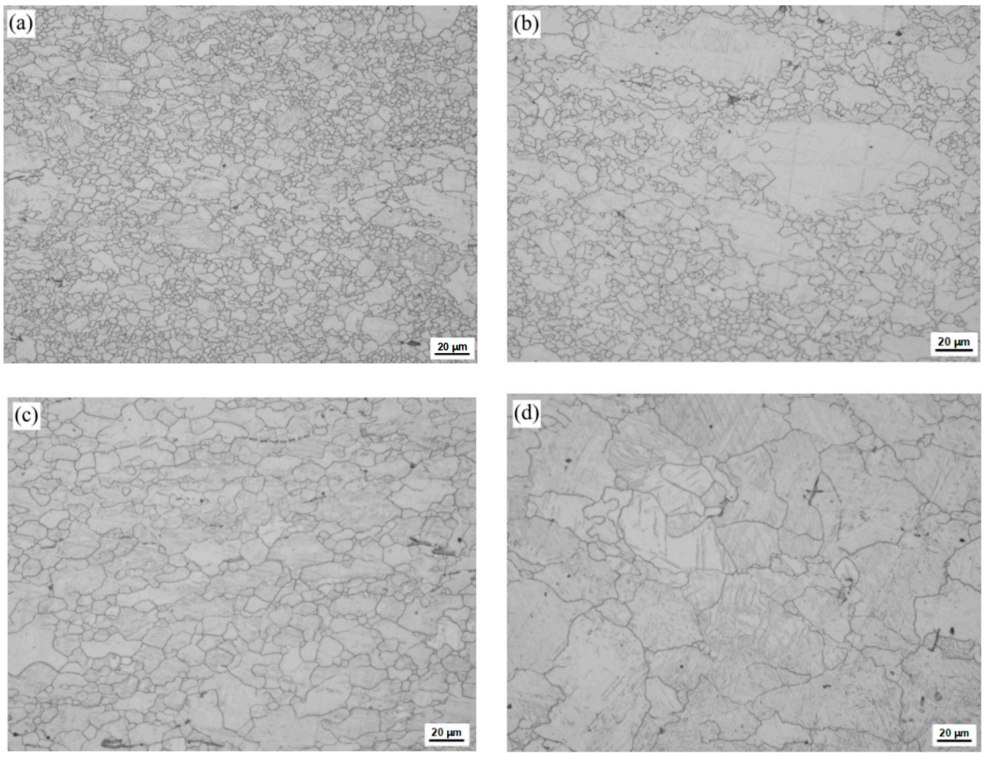


Figure 7. Microstructure photograph of AZ31B alloy with different strain rates and deformation temperatures: (**a**) $T = 623\ K$, $\dot{\varepsilon} = 0.1\ s^{-1}$; (**b**) $T = 673\ K$, $\dot{\varepsilon} = 0.1\ s^{-1}$; (**c**) $T = 773\ K$, $\dot{\varepsilon} = 0.1\ s^{-1}$; (**d**) $T = 773\ K, \dot{\varepsilon} = 10\ s^{-1}$.

It can be seen from the figure that there are a large number of fine, recrystallized grains in Figure 7a,b, as well as large original grains with relatively large sizes, but the degree of dynamic recrystallization in Figure 7a is significantly higher. Therefore, the strain rate sensitivity index is higher when the deformation temperature is 623 K and the strain rate is

0.1 s^{-1}. A previous study [27] also found that the strain rate sensitivity index gradually decreased with the increase in grain size.

It can be seen from the comparison of Figure 7c,d that the strain rate sensitivity index gradually decreased with the increase in strain rate. This can be explained well by the change in the microstructure in Figure 7; that is, under the same deformation temperature, with the increase in the strain rate, the grain size of the AZ31B magnesium alloy gradually increased, which led to the decrease in the strain rate sensitivity index.

3.3. Strain Hardening Exponent

The strain hardening index n reflects the ability of metal materials to resist uniform plastic deformation and is the performance index used to characterize the work hardening behavior of metal materials. H. P. Stüwe et al. [28] pointed out that the strain hardening exponent n is caused by the mutual balance between the strain hardening and softening mechanisms. The calculation formula for the strain hardening exponent n used in this study was as follows [29]:

$$n = \left.\frac{d\log\sigma}{d\log\varepsilon}\right|_{\dot{\varepsilon},T} \tag{4}$$

where n is the strain hardening index; σ is the flow stress (MPa); $\dot{\varepsilon}$ is the strain rate (s^{-1}); ε is the strain; and T is the deformation temperature (K). It can be seen from Equation (1) that, when the material deforms, the strain hardening index depends on its internal range (strain interval); that is, the variable is $\Delta\varepsilon$. Under the same strain rate and temperature conditions, the larger the strain interval, the larger the denominator and the smaller the strain hardening index n. The results show that the strain hardening strength of AZ31B magnesium alloy decreased with the increase in strain; that is, with the deepening of deformation, AZ31B magnesium alloy gradually changed from work hardening to softening.

Figure 8 shows the variation in the strain hardening index of AZ31B magnesium alloy with deformation conditions (deformation temperature and deformation amount) under different strain rates. The drawing method is similar to Figure 6.

It can be seen from the figure that, under different strain rates, the strain hardening exponent of AZ31B magnesium alloy was almost positive when the strain was small; that is, at the early stage of deformation, the work hardening effect of AZ31B magnesium alloy played a dominant role in the deformation process. This was because the dislocation density increased rapidly at the beginning of deformation and the distortion energy was also high, which meant that the alloy material was in the working hardening state, and the strain hardening index was positive. Moreover, the strain hardening index of AZ31B magnesium alloy decreased with the increase in strain, which indicated that, with the deepening of deformation, AZ31B magnesium alloy gradually changed from work hardening to softening.

Figure 8 further shows that the peak value of the strain hardening index of AZ31B magnesium alloy occurs at low deformation and low temperature, and the peak value of the strain hardening index and the work hardening region gradually increased with the increase in the strain rate, up to 0.32. Combined with Figure 5, this shows that the flow stress in the alloy increased with the increase in the strain rate, which also fully reflected the change in the strain hardening index of the alloy with the strain rate.

Figure 9 shows the effects of different deformation conditions on the microstructure of AZ31B magnesium alloy. It can be seen from the figure that the strain hardening index of AZ31B magnesium alloy gradually decreased with the increase in deformation temperature. This can be explained well by the change law for the microstructure. As shown in the figure, as the deformation temperature increased, the grain size of AZ31B magnesium alloy gradually increased; that is, the nucleation and growth of recrystallized grains involved a great number of dislocations and variable properties, resulting in a decrease in the n value.

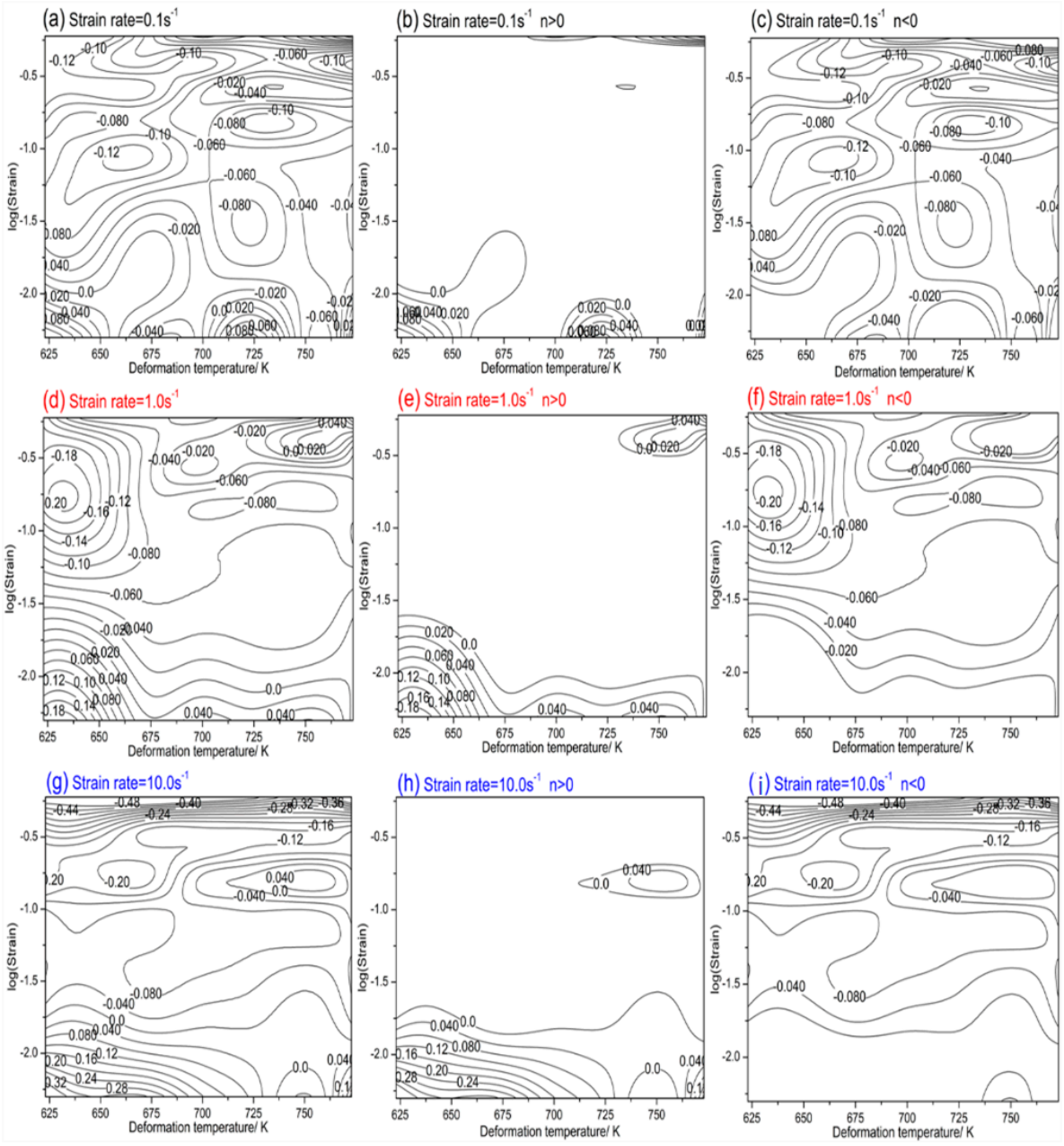


Figure 8. Contour map of strain hardening exponent of AZ31B mg alloy under different strain rate conditions: (**a**–**c**) $\dot{\varepsilon} = 0.1\ s^{-1}$; (**d**–**f**) $\dot{\varepsilon} = 1\ s^{-1}$; (**g**–**i**) $\dot{\varepsilon} = 10\ s^{-1}$.

In addition, the strain hardening index at 773 K and a strain rate of 0.1 s^{-1} was smaller than that at 773 K and a strain rate of 1 s^{-1}. This was because, as the strain rate increased, the time required for the material to produce the same deformation decreased, resulting in insufficient time for the material to complete the nucleation and growth of dynamic recrystallization during deformation, which made the material harden. Therefore, the strain hardening index was also large when the strain rate was large.

This can also be explained by the change in the microstructure. It can be seen from Figure 9 that the grain size at the strain rate of 0.1 s^{-1} was significantly larger than that at the strain rate of 1 s^{-1}. Combined with the above description, under the condition shown in Figure 9c, the recrystallized grains grew significantly and the ability of metal materials to resist uniform plastic deformation decreased, which made the n value decrease at this time.

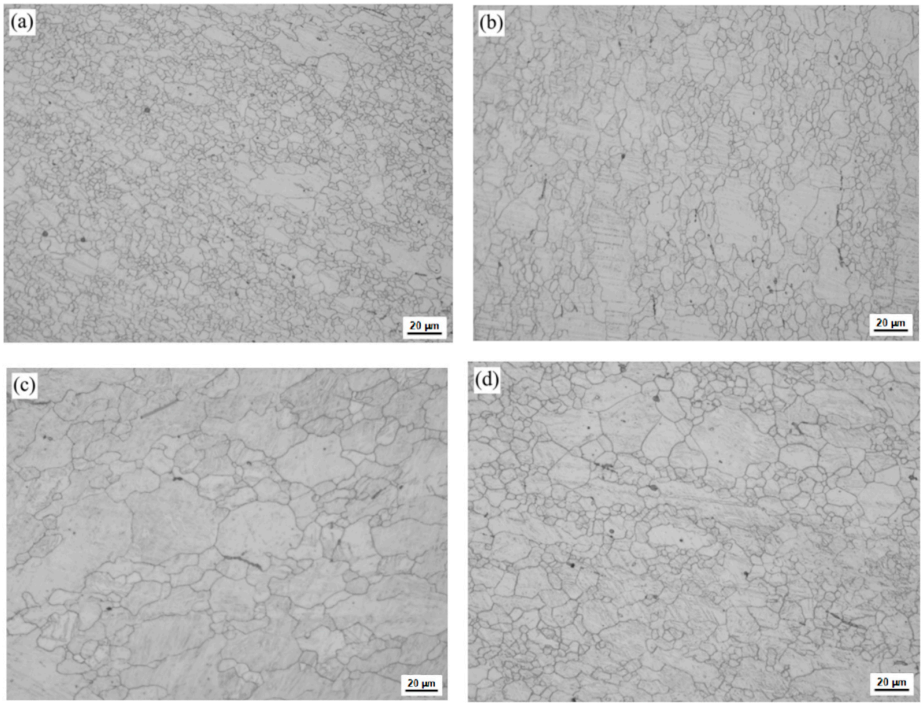


Figure 9. Microstructure photograph of AZ31B alloy under different strain rates and deformation temperatures: (**a**) $T = 648\ K, \dot{\varepsilon} = 0.1\ s^{-1}$; (**b**) $T = 698\ K, \dot{\varepsilon} = 0.1\ s^{-1}$; (**c**) $T = 773\ K, \dot{\varepsilon} = 0.1\ s^{-1}$; (**d**) $T = 773\ K, \dot{\varepsilon} = 1\ s^{-1}$.

4. Conclusions

The hot deformation behavior of as-cast AZ31B magnesium alloy was studied at 623~773 K; strain rates of 0.1 s^{-1}, 1 s^{-1}, 10 s^{-1}; and 60% strain. It was found that the flow stress of as-cast AZ31B magnesium alloy was highly sensitive to deformation temperature, strain rate, and strain. The strain rate sensitivity index m and strain hardening index n of AZ31B magnesium alloy were studied in depth, as shown in the following conclusions:

1. The flow stress of as-cast AZ31B magnesium alloy decreased with the decrease in the strain rate, the increase in the strain, and the increase in the deformation temperature. With the increase in the degree of deformation and the temperature of the magnesium alloy, recrystallization softening gradually occupied the dominant position, and the influence of the strain rate on the flow stress was gradually reduced;
2. The strain rate sensitivity index m was affected by the amount of strain, the strain rate, the deformation temperature, and the grain size as follows. Firstly, the strain rate sensitivity index m of AZ31B magnesium alloy gradually decreased with the increase in the strain rate and particle size. Secondly, the peak m of the strain rate sensitivity index appeared in the low strain rate region, decreased, and then increases with the increase in strain. In addition, the strain rate sensitivity index m decreased with increasing temperature until it was almost unaffected by temperature (above 700 K);
3. The strain hardening exponent n was affected by the strain and strain rate, the deformation temperature, and the grain size as follows. Firstly, at different strain rates, the positive strain hardening indexes of AZ31B magnesium alloy almost all appeared in the small strain region. In addition, the strain hardening index of AZ31B magnesium alloy decreased with the increase in the strain, temperature, and particle size but increased with the increase in the strain rate. Finally, the peak value of the strain hardening strength of AZ31B magnesium alloy gradually increased with the increase in the strain rate.

Author Contributions: Conceptualization: Y.Z. and Z.H.; methodology, Y.Z. and Q.W.; software, L.Q.; validation, Y.Z., Q.W. and Z.L.; formal analysis, Z.L.; investigation, Q.W.; resources, L.M. and L.Q.; data curation, Y.Z.; writing—original draft preparation, Y.Z.; writing—review and editing, Q.W.; visualization, Y.Z.; supervision, Z.H.; project administration, L.M.; All authors have read and agreed to the published version of the manuscript.

Funding: Shanxi Province Key R&D Project (201903D121088), Shanxi Graduate Innovation Project (2021Y673), Basic Research Program of Shanxi Province, (202203021211208), and General Program of National Natural Science Foundation of China, (52075357).

Institutional Review Board Statement: Not applicable.

Informed Consent Statement: Not applicable.

Conflicts of Interest: The authors declare no conflict of interest.

References

1. Chen, Z.; Xia, W.; Yan, H.; Li, X.; Cheng, Y.; Guo, Q.; Chen, D. *Wrought Magnesium Alloys*; Chemical Industry Press: Beijing, China, 2005; p. 239.
2. Aghion, E.; Bronfin, B.; Eliezer, D. The role of the magnesium industry in protecting the environment. *J. Mater. Process. Technol.* **2001**, *117*, 381–385. [CrossRef]
3. Huang, G.; Qian, B.; Wang, L.; Jonas, J.J. Study on the critical conditions for initial dynamic recrystallization of AZ31 magnesium alloy. *Rare Met. Mater. Eng.* **2007**, *36*, 2080–2083. [CrossRef]
4. Tsao, L. Evaluation of superplastic formability of the AZ31 magnesium alloy. *Int. J. Mater. Res.* **2001**, *92*, 572–577. [CrossRef]
5. Jian, T.; Zhang, S. On the 1012 twinning growth mechanism in hexagonal close-packed metals. *Mater. Des.* **2016**, *96*, 143–149. [CrossRef]
6. Wang, H.; Sun, X.; Kurukuri, S.; Worswick, M.J.; Li, D.Y.; Peng, Y.H.; Wu, P.D. The strain rate sensitive and anisotropic behavior of rare-earth magnesium alloy ZEK100 sheet. *J. Magnes. Alloy.* 2021; *in press*. [CrossRef]
7. Karimi, E.; Zarei-Hanzaki, A.; Pishbin, M.H.; Abedi, H.R. Changizian, Instantaneous strain rate sensitivity of wrought AZ31 magnesium alloy. *Mater. Des.* **2013**, *49*, 173–180. [CrossRef]
8. Sriraman, N.; Kumaran, S.; Sathiya Narayanan, N. Influence of thermomechanical processing on microstructure, mechanical and strain hardening properties of single-phase Mg-4Li-0.5Ca alloy for structural application. *J. Magnes. Alloy.* **2020**, *8*, 1262–1268. [CrossRef]
9. Zhang, R.; Yang, L.; Liu, Q. Frequency Mapping Analysis Based on KAM Theory. *J. Inn. Mong. Univ. Nat. Sci. Ed.* **2013**, *44*, 239–243.
10. Shoichiro, Y.; Hisashi, N.; Hirokuni, Y.; Manabe, K. Formability enhancement in magnesium alloy stamping using a local heating and cooling technique: Circular cup deep drawing process. *J. Mater. Process. Technol.* **2003**, *142*, 609–613. [CrossRef]
11. Chen, F.-K.; Huang, T.-B.; Chang, C.-K. Deep drawing of square cups with magnesium alloy AZ31 sheets. *Int. J. Mach. Tools Manuf.* **2003**, *43*, 1553–1559. [CrossRef]
12. Barnett, M.R. Influence of deformation conditions and texture on the high temperature flow stress of magnesium AZ31. *J. Light Met.* **2001**, *1*, 167–177. [CrossRef]
13. Nave, M.D.; Barnett, M.R. Microstructures and textures of pure magnesium deformed in plane-strain compression. *Scr. Mater.* **2004**, *51*, 881–885. [CrossRef]
14. Spigarelli, S.; El Mehtedi, M.; Cabibbo, M.; Evangelista, E.; Kaneko, J.; Jäger, A.; Gartnerova, V. Analysis of high-temperature deformation and microstructure of an AZ31 magnesium alloy. *Mater. Sci. Eng. A* **2007**, *462*, 197–201. [CrossRef]
15. Ding, X.F.; Shuang, Y.H.; Lin, W.L.; Zhang, J. Study on the flow behavior and constitutive model of extruded magnesium alloy. *J. Plast. Eng.* **2017**, *24*, 165–171. [CrossRef]
16. Tsao, L.; Huang, Y.T.; Fan, K.H. Flow stress behavior of AZ61 magnesium alloy during hot compression deformation. *Mater. Des.* **2014**, *53*, 865–869. [CrossRef]
17. Spigarelli, S.; Jäger, A.; El Mehtedi, M.; Gärtnerová, V. Microstructural and constitutive analysis in process modeling of hot working: The case of a Mg-Zn-Mn alloy. *Mater. Sci. Eng. A* **2016**, *661*, 40–50. [CrossRef]
18. Zhou, J.; Wu, R.; Yuan, C.; Jiao, W.; Li, T. Deformation Behavior of AZ31B Magnesium Alloys with Different Process States under Thermal Compression AZ31B. *Rare Met. Mater. Eng.* **2020**, *49*, 1793–1798.
19. Zhang, Q.; Wang, Y.; Ping, L.I.; Zhu, L.M.; Quan-An, L.I. Hot compression behavior of AZ81-0.5Sb magnesium alloy. *Trans. Mater. Heat Treat.* **2019**, *40*, 54–58. [CrossRef]
20. Lin, J.; Chen, M.S.; Zhong, J. Prediction of 42CrMo steel flow stress at high temperature and strain rate. *Mech. Res. Commun.* **2008**, *35*, 142–150. [CrossRef]
21. Wang, G.; Hui, S.X.; Wen-Jun, Y.E. Hot compressive behavior of Ti-3.0Al-3.7Cr-2.0Fe-0.1B titanium alloy. *Trans. Nonferrous Met. Soc. China* **2012**, *22*, 2965–2971. [CrossRef]
22. Luo, J.; Li, M.Q. Strain rate sensitivity and strain hardening exponent during the isothermal compression of Ti60 alloy. *Mater. Sci. Eng. A* **2012**, *538*, 156–163. [CrossRef]

23. Wang, Y.; Gong, B.; Li, B.; Song, B. Behavior of H62 Brass Alloy Hot Deformation. *Nonferrous. Met.* **2010**, *62*, 11–14. [CrossRef]
24. Zhao, X.; Qiao, J.; Chen, J. Hot Compression Behavior of 6061 Aluminum Alloy. *Hot Work. Technol.* **2009**, *38*, 10–12. [CrossRef]
25. Otsuka, M.; Tsurumaki, K.I.; Niimura, M.; Horiuchi, R. Superplasticity in an Al-Li-Cu-Mg-Zr alloy. *J. Jpn. Inst. Light Met.* **1986**, *36*, 752–758. [CrossRef]
26. Luo, J.; Li, M.; Yu, W.; Li., H. The variation of strain rate sensitivity exponent and strain hardening exponent in isothermal compression of Ti–6Al–4V alloy. *Mater. Des.* **2010**, *31*, 741–748. [CrossRef]
27. Hu, S. Study on Grain Size Effect of Microstructure and Mechanical Properties of Pure Copper. Master's Thesis, Nanjing University of Technology, Nanjing, China, 2016. [CrossRef]
28. Stüwe, H.P.; Les, S. Strain rate sensitivity of flow stress at large strains. *Acta Mater.* **1998**, *46*, 6375–6380. [CrossRef]
29. El-Domiaty, A. The effect of strain, strain rate and temperature on formability of Ti-6Al-4V alloy. *J. Mater. Process. Technol.* **1992**, *32*, 243–251. [CrossRef]